Spectral shaping for non-Gaussian source spectra in optical coherence tomography

Renu Tripathi

Department of Electrical Engineering and Computer Science, Massachusetts Institute of Technology, 77 Massachusetts Avenue, Cambridge, Massachusetts 02139

Nader Nassif and J. Stuart Nelson

Beckman Laser Institute and Medical Clinic, University of California at Irvine, 1002 Health Sciences Road East, Irvine, California 92612

Boris Hyle Park and Johannes F. de Boer

Harvard Medical School and Wellman Labs for Photomedicine, Massachusetts General Hospital, 50 Blossom Street, BAR 724, Boston, Massachusetts 02114

Received October 1, 2001

We present a digital spectral shaping technique to reduce the sidelobes (ringing) of the axial point-spread function in optical coherence tomography for non-Gaussian-shaped source spectra. The spectra of two superluminescent diodes were combined to generate a spectrum with significant modulation. Images of onion cells demonstrate the improved image quality in a turbid biological sample. A quantitative analysis of the accompanying penalty in signal-to-noise ratio is given.

OCIS codes: 170.4500, 170.3010, 170.0170, 110.4850, 120.5050.

In optical coherence tomography[1,2] (OCT) the temporal coherence or, equivalently, the source spectral bandwidth governs the axial point-spread function. To increase axial resolution, several methods have been used to generate light with low temporal and high spatial coherence.[3–8] In virtually all these methods special care must be taken to generate spectral shapes that resemble a Gaussian profile. Non-Gaussian spectral shapes will result in the presence of sidelobes in the coherence envelope that will generate spurious structures in OCT images. Many sources that can be used for OCT (e.g., erbium-doped fiber amplifiers and self-phase-modulated spectral broadening of short pulses in microstructure fibers[9]) do not have Gaussian spectra and therefore require some form of spectral filtering[3,5] or shaping of the source spectrum into a smoother form.[8] In this Letter we demonstrate that these problems can be addressed by a signal processing algorithm without significant penalty to the signal-to-noise ratio.

Digital signal processing was previously used to increase resolution. Kulkarni *et al.*[10] demonstrated this in a two-dimensional image by an iterative deconvolution with the coherence envelope's point-spread function in the space domain, but this method is computationally intensive. Bashkansky *et al.*[11] proposed spectral shaping to improve the measured cross-correlation function. Using a virtually Gaussian source spectrum, they demonstrated an increase in resolution of a single depth profile of two glass slides pressed together by deconvolution with the measured power spectrum in the Fourier domain. However, this method for increasing spatial resolution increases the noise floor significantly.

In this Letter we focus on the reduction of spurious structures in OCT images that have been caused by sidelobes. Previously, sidelobe reduction in a single depth profile of a glass slide was demonstrated.[12] Here we present, for the first time to our knowledge, the spectral shaping technique applied to imaging of biological structure by use of a source spectrum with significant modulation and analyze the penalty in signal-to-noise ratio that is incurred.

In an OCT system the coherence function is proportional to the Fourier transform of source spectrum $S(k)$:

$$I(\Delta z) \propto \mathrm{Re} \int \exp(ik\Delta z) S(k) \mathrm{d}k , \qquad (1)$$

where $k = 2\pi/\lambda$ is the free-space wave number and $\Delta z = z - z'$ is the path-length difference between reference and sample waves.

The spectral shaping technique shapes the source spectrum by Fourier transforming the interferometric signal in relation (1) and then applying a correction to each Fourier component such that the spectrum becomes Gaussian. After an inverse transform, the ideal coherence function for a Gaussian source spectrum is obtained.

The experimental setup is similar to that reported in Ref. 13, except that in the current setup the design wavelength was 830 nm and no phase modulator was employed. Light from two orthogonally polarized superluminescent diodes (SLDs; SLD-371 and SLD-381, Superlum, Moscow, Russia) was coupled into a single-mode fiber after power efficient combination by a polarizing beam splitter. The individual spectra were in orthogonal states and the source power after combination was 0.9 mW for SLD 1 and 0.3 mW for SLD 2. Source light was then split equally into the sample and reference arms by a fiber 2×2 coupler. Axial scanning over 2 mm in depth was done with a rapid scanning optical delay line,[14] resulting in 500 A

0146-9592/02/060406-03$15.00/0

lines per second and a 400-kHz center frequency of the interference fringes. In the detection arm, light was split into orthogonal polarization states before being detected. The polarization controller in the detection arm was aligned such that half of the light from each individual source reflected from the reference arm was sent to each detector, ensuring that each detector sensed the same combination of individual spectra. The polarization controller in the sample arm was aligned to achieve the same objective for sample-arm light. The detector signals were digitized with a dual-channel 12-bit, 5-MHz analog-to-digital conversion board. The sample arm's focal diameter was 25 μm. The sources exhibited a noise peak at 250 kHz, close to the carrier frequency. The fringes detected in the two orthogonal polarization channels were approximately 90° out of phase owing to fiber birefringence. We exploited this phase difference to implement balanced detection by subtracting the orthogonal polarization channels, which significantly reduced the 250-kHz noise peak without reducing the signal, resulting in virtually shot-noise-limited detection. However, significant sample birefringence would pose a problem in this nonideal balanced detection scheme.

In Figure 1 the combined spectrum of SLD1 and SLD2 is shown. We calculated the spectrum from the average of the square root of the power spectrum of 500 A-lines (10,000 samples per A-line, zero padded to 16,384) by Fourier transforming the interferometric responses to a single surface. The dashed curve is a Gaussian fit with a center wavelength of 833 nm and a FWHM of 49 nm to the spectrum, determined by the zeroth, first, and second moments of the spectral density. The ratio of this ideal Gaussian source spectrum and the measured spectral density defines a spectral correction curve, SC(λ). We obtained the spectrally filtered response of each depth profile by multiplying the Fourier transform of each individual depth profile by SC(λ) and performing the inverse transform. The coherence function envelope was obtained by digital quadrature demodulation with a spatial resolution of 1.6 μm.

Figure 2 shows the coherence envelope before and after spectral shaping for a single surface (glass slide) and the sibelobe reduction at specific locations. The increase in the noise floor far from the coherence envelope was 8.5 dB, and the FWHM of the coherence envelope was 6.0–6.5 μm.

To demonstrate that spectral shaping is not only feasible for (highly) reflective single surfaces but actually improves images of biological structures, we imaged a section of an onion's skin. A total of six images were acquired at the same location. It took 1 s to acquire each image, scanning a width of 1 mm, and each image was processed both without and with spectral shaping. To obtain the SC(λ) for each individual image we determined the source spectral density from the image data by calculating the square root of the power spectrum for each A-line in the image and averaging over all A-lines (500). We used the zeroth moment of this spectral density and the first and second moments of the glass slide's spectral density to determine the ideal Gaussian source spectrum. As can be seen from Fig. 1, the spectral density as determined from one image is a good approximation of the glass slide's spectrum. The image spectrum was scaled vertically such that the ideal Gaussians for the spectra of the image and of the glass slide exactly overlapped.

Figure 3 shows side by side the uncorrected and the spectrally shaped images after the six individual images have been summed to reduce background noise. Both images were gray-scale coded over a dynamic range of 40 dB (from maximum signal in the image to the noise level) and cropped to 600 μm $\times$ 480 μm (width $\times$ depth). The image was magnified in the depth direction by a factor of 2 to increase the visibility of the sidelobes. Processing data acquired in 1 s required 2 s on a 1.3 GHz Pentium IV processor.

Throughout the image, spurious structures were visible about strongly scattering objects that correspond to the positions of the sibelobes. The spectrally shaped image showed a significant reduction of these spurious structures. Figure 4 shows single depth profiles averaged over four A-lines before and after spectral correction and the sidelobe reduction achieved in the area that lies between the arrows in Fig. 3. The increase in the noise floor determined by averaging of the signal in the air above the sample surface was only 0.9 dB.

Increase in the noise floor can be estimated as follows: The intensity reflected from the sample arm is proportional to the square of the interferometric intensity, $I(z)$ in relation (1). Curve SC(λ) gives a multiplication factor for each Fourier component $f(\lambda)$,

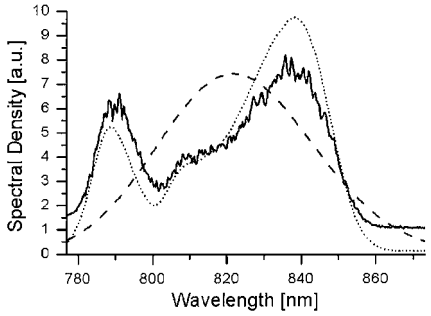

Fig. 1. Spectra and Gaussian fit. Dotted curve, spectrum determined from glass slide reflection; Solid curve, spectrum determined from a single image; dashed curve, Gaussian fit to each spectrum.

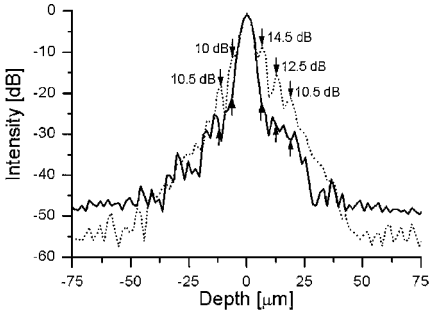

Fig. 2. Coherence envelopes determined from glass slide reflection. Dotted curve, uncorrected response; solid curve, spectrally corrected response. Arrows indicate locations of calculated sidelobe suppression.

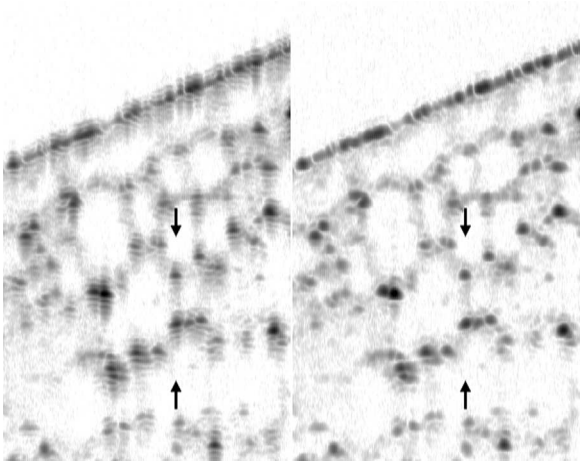

Fig. 3. Images of onion cells before and after spectral shaping. The image size was 600 μm $\times$ 480 μm (width $\times$ depth). Gray-scale code from 0 dB (maximum signal in image) to -40 dB (noise floor). Left, uncorrected image; right, image after spectral shaping. Arrows indicate the location of the depth profile shown in Fig. 4.

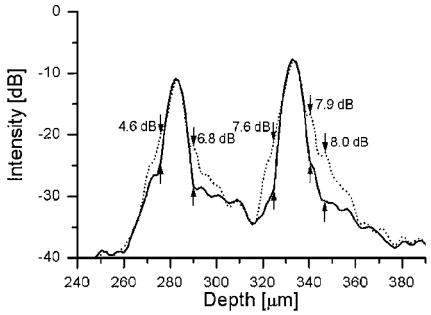

Fig. 4. Depth profiles for the onion sample. Dotted curve, uncorrected response; solid curve, spectrally corrected response. Arrows indicate locations of calculated sidelobe suppression. The vertical axis is calibrated to the gray scale in Fig. 3. The horizontal scale shows depth with respect to the top of the image.

which consists of a signal $f_s(\lambda)$ and a noise $f_n(\lambda)$ contribution. From Parseval's theorem, the average noise level $\langle I_n^2(z)\rangle$ is equal to $\langle |f_n(\lambda)|^2\rangle$, where angle brackets denote averaging. Thus the increase in the noise level is given by $\int \mathrm{SC}^2(\lambda)\,|f_n(\lambda)|^2 \mathrm{d}\lambda / \int |f_n(\lambda)|^2 \mathrm{d}\lambda$, which, assuming a white-noise spectrum, reduces to $10 \log\langle \mathrm{SC}^2(\lambda)\rangle$ in decibels. For the glass slide we calculated a value of 8.65 dB, which corresponds well to a measured value of 8.5 dB, and for the image we calculated a value of 0.97 dB, which corresponds well to a measured value of 0.9 dB. The 8.5-dB increase in the noise level for the glass slide is due mainly to the large value of $\mathrm{SC}(\lambda)$ from 855 to 867 nm (Fig. 1).

The peak values of the coherence envelopes are proportional to $\int |f_s(\lambda)| \mathrm{d}\lambda$. Equal peak heights before and after spectral shaping are maintained if $\int |f_s(\lambda)| \mathrm{d}\lambda = \int \mathrm{SC}(\lambda)\,|f_s(\lambda)| \mathrm{d}\lambda$. This condition can be approximately satisfied by use of the zeroth moment of the spectral density $|f(\lambda)|$ as the zeroth moment for the ideal Gaussian. Doing so results in virtually equal values of the coherence peaks for uncorrected and spectrally filtered depth profiles, as can observed from Figs. 2 and 4. The optimal choice of the first and second moments for the ideal Gaussian in a particular measurement can be determined by choice of the maximum allowable increase in the noise floor.

Absorption- and wavelength-dependent scattering will alter the reflected spectrum and thus the coherence function in all OCT systems. To some extent, spectral shaping is able to correct for these effects on the coherence function, because the average reflected spectrum is used as a source reference. However, the method is not able to correct for changes in the reflected spectrum as a function of depth. In conclusion, the spectral shaping procedure enables non-Gaussian source spectra to be used in OCT, which simplifies the development of low-cost broadband sources.

Research grants from the National Institutes of Health (EY 12877 and GM 58785), the Whitaker Foundation (26083), the U.S. Office of Naval Research (N00014-94-1-0874), and the U.S. Department of Energy are gratefully acknowledged. J. F. de Boer's e-mail address is deboer@helix.mgh.harvard.edu.

References

1. D. Huang, E. A. Swanson, C. P. Lin, J. S. Schuman, W. G. Stinson, W. Chang, M. R. Hee, T. Flotte, K. Gregory, C. A. Puliafito, and J. G. Fujimoto, Science **254,** 1178 (1991).
2. A. F. Fercher, J. Biomed. Opt. **1,** 157 (1996).
3. W. Drexler, U. Morgner, F. X. Kartner, C. Pitris, S. A. Boppart, X. D. Li, E. P. Ippen, and J. G. Fujimoto, Opt. Lett. **24,** 1221 (1999).
4. A. F. Fercher, C. K. Hitzenberger, M. Sticker, E. Moreno-Barriuso, R. Leitgeb, W. Drexler, and H. Sattmann, Opt. Commun. **185,** 57 (2000).
5. I. Hartl, X. D. Li, C. Chudoba, R. K. Ghanta, T. H. Ko, J. G. Fujimoto, J. K. Ranka, and R. S. Windeler, Opt. Lett. **26,** 608 (2001).
6. J. M. Schmitt, S. L. Lee, and K. M. Yung, Opt. Commun. **142,** 203 (1997).
7. A. Baumgartner, C. K. Hitzenberger, H. Sattmann, W. Drexler, and A. F. Fercher, J. Biomed. Opt. **3,** 45 (1998).
8. Y. Zhang, M. Sato, and N. Tanno, Opt. Lett. **26,** 205 (2001).
9. J. Ranka, R. S. Windeler, and A. J. Stentz, Opt. Lett. **25,** 25 (2000).
10. M. D. Kulkarni, C. W. Thomas, and J. A. Izatt, Electron. Lett. **33,** 1365 (1997).
11. M. Bashkansky, M. D. Duncan, J. Reintjes, and P. R. Battle, Appl. Opt. **37,** 8137 (1998).
12. J. F. de Boer, C. E. Saxer, and J. S. Nelson, Appl. Opt. **40,** 5787 (2001).
13. C. E. Saxer, J. F. de Boer, B. H. Park, Y. Zhao, Z. Chen, and J. S. Nelson, Opt. Lett. **25,** 1355 (2000).
14. G. J. Tearney, B. E. Bouma, and J. G. Fujimoto, Opt. Lett. **22,** 1811 (1997).